Dual-Readout Calorimetry for High-Quality Energy Measurements

Progress Report

Presented by:

Dr. Gabriella Gaudio and Dr. Richard Wigmans[1]

on behalf of the RD52 (DREAM) Collaboration

(Cagliari - Cosenza - Iowa State - Pavia - Pisa - Roma I - Texas Tech)

3 April 2012

[1]Contact person. Tel. [806] 742 3779, FAX [806] 742 1182, E-mail: wigmans@ttu.edu

1 Introduction

On August 31, 2011, the CERN Research Board decided to accept the DREAM Collaboration's detector R&D proposal [1] and included it as project RD52 in its official scientific program. This document constitutes the first RD52 progress report. In this report, we describe our activities since the last time we reported to the SPS Committee (June 11, 2011), as well as our future plans.

In 2011, we were allocated 24 days of test beam in the SPS H8 beam. We used this time to

1. Install and commission the new beam definition system we developed for our tests
2. Tune the particle beams needed for our purpose, especially electron beams
3. Measure the performance of a dedicated matrix of molybdenum doped $PbWO_4$ crystals
4. Measure the polarization characteristics of the light produced in a BSO crystal as a function of the (em) shower depth
5. Perform extensive tests of the first two modules of our new dual-readout fiber calorimeter (SuperDREAM)

These activities have led to two papers, which have either already been accepted or are about to be submitted for publication, namely:

1. N. Akchurin *et al.*, *Detection of electron showers in Dual-Readout crystal calorimeters*, accepted for publication in Nucl. Instr. and Meth. (March 2012)
2. N. Akchurin *et al.*, *On the production of coherent light in electromagnetic showers developing in crystal calorimeters*, soon to be submitted to Nucl. Instr. and Meth. (March 2012)

In addition, a number of internal notes about ongoing data analyses were completed. All RD52 publications can be found on the official web page:
http://highenergy.phys.ttu.edu/dream/results/publications/publications.html

In the following sections, we elaborate on these activities.

2 Test beam optimization

In any calorimeter R&D project, good quality electron beams are of great importance. Electrons are essential for calibrating the individual calorimeter cells, and for checking the linearity of the calorimeter readout. Moreover, electrons are the most sensitive tools to check the response uniformity.

Setting up good quality electron beams is notoriously difficult in the H8 beam. The quality of the beams delivered to our experimental area was unfortunately not good enough. Therefore, we have had to invest quite a bit of time into this ourselves. Another complicating factor is the

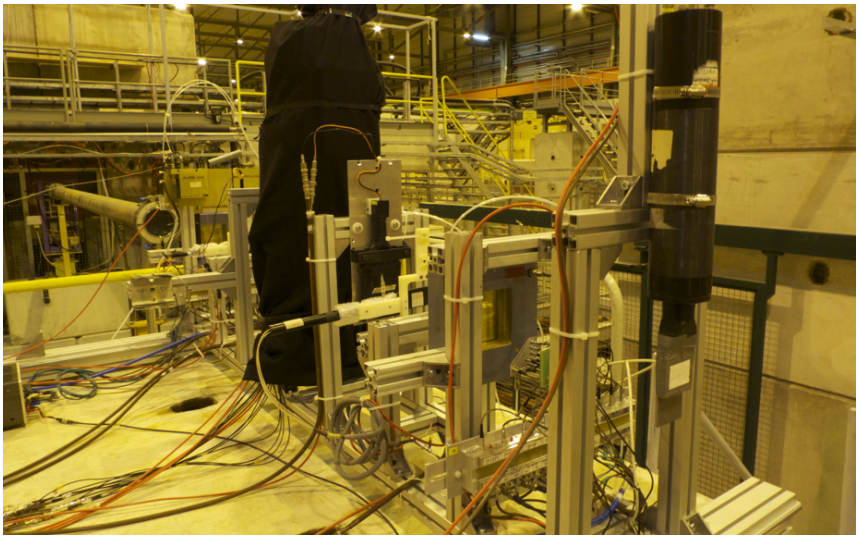

Figure 1: The new, moveable system of trigger and beam definition counters installed upstream of the calorimeter.

fact that experiments downstream from our setup (TOTEM, CALICE) also use the H8 beam line. Our equipment has to be moved out of the way to make this possible.

For this reason, we have built a system of trigger counters and beam defining elements that can be moved in and out of the beam line in a reproducible fashion. This system consists of two small trigger counters, a veto counter consisting of a scintillator paddle with a circular hole, two wire chambers, a fiber hodoscope and a preshower detector (PSD). All these elements are mounted on a rail that can be moved sideways to give passage to the beam (Figure 1). The calorimeters themselves are placed on a table that can be lowered.

Another crucial component of our particle identification system is a muon counter, a 50×50 cm^2 scintillator paddle located in a fixed position more than 20 m downstream, behind more than 10 nuclear interaction lengths of absorber material.

Because of the poor quality of the electron beams delivered by the SPS in the H8C area, our particle identification system based on auxiliary detectors turned out to be crucially important. This is illustrated in Figure 2 for the 20 GeV electron beam. The signal distribution for the raw data (Figure 2a) is dominated by contaminating muons. After eliminating these, an additional contribution from pions becomes visible (Figure 2b). These could be effectively recognized and eliminated with the PSD and we ended up with a clean sample of electron events (Figure 2c). Even though the event rates were very low, especially at low energies, useable beams could be obtained in this way.

3 Tests with crystals

Our interest in studying high-Z scintillating crystals for the purpose of dual-readout calorimetry derived from the potential reduction of the contribution of stochastic fluctuations to the energy resolution of such calorimeters. In the fiber calorimeter with which the benefits of dual-readout calorimetry were first demonstrated [2], the contribution of such fluctuations was $\sim 40\%/\sqrt{E}$,

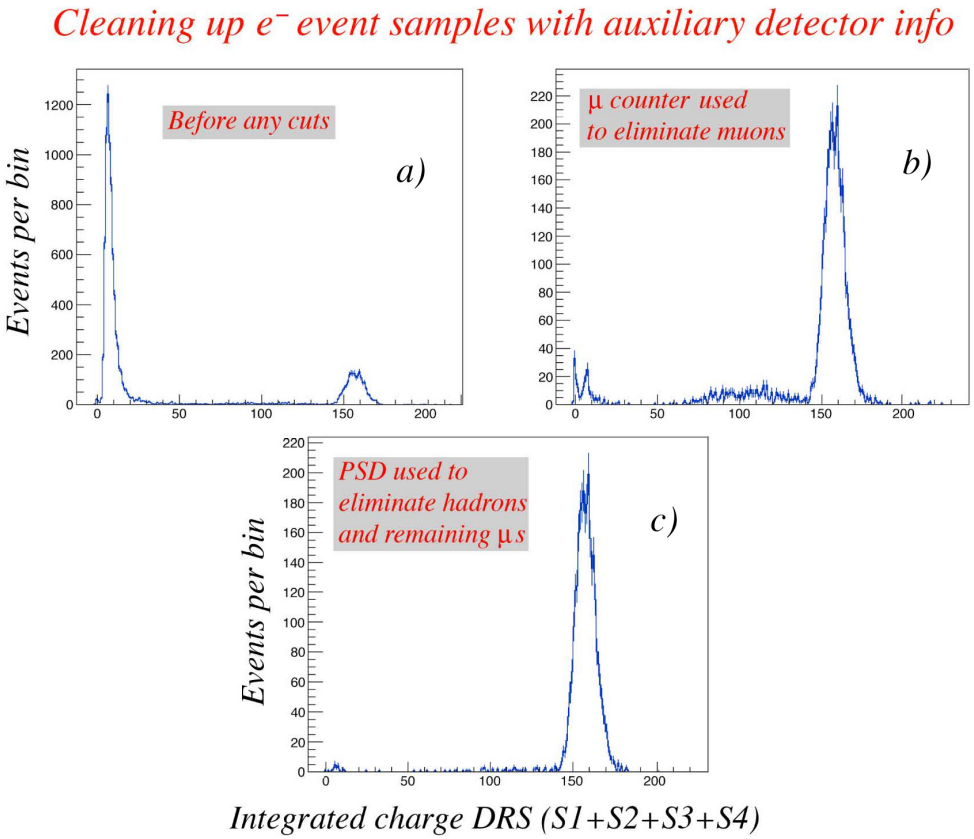

Figure 2: Particle identification in H8, for a 20 GeV electron beam heavily contaminated with muons and (to a less extent) pions. See text for details.

with approximately equal contributions ($\sim 30\%/\sqrt{E}$) from sampling fluctuations and from Čerenkov photoelectron statistics. Our goal in further developing this experimental technique is to reduce the contribution of stochastic fluctuations to the point where these are comparable to the irreducible effects of fluctuations in visible energy, estimated at $\sim 15\%/\sqrt{E}$. Crystals were believed to offer good opportunities in this respect.

Calorimeters consisting of high-Z scintillating crystals are the detectors of choice in particle physics experiments that aim for the best energy resolution in electron and γ detection. Examples of recent experiments using such calorimeters include BaBar at SLAC [4], Belle at KEK [5], L3 at LEP [3] and CMS at the LHC [6]. However, our goals are different from those in the mentioned experiments, in the sense that we want to use crystals for dual-readout purposes, in order to achieve superior *hadronic* calorimeter performance. The question is then if and to what extent crystals optimized for this purpose can at the same time also be excellent em calorimeters.

In recent years, we have developed four different methods to split crystal signals into their scintillation and Čerenkov components [7, 8, 9, 10, 11, 12]. These methods exploit

1. differences in the angular distribution of the light [7],

2. differences in the spectral characteristics [8],

3. differences in the time structure of the signals [8], and

4. the fact that Čerenkov light is polarized, while scintillation light is not [11].

All these studies were carried out with high-energy muons, pions or electrons that traversed a single crystal. In our most recent paper, we investigate to what extent the promise of improved calorimeter performance can be realized with such crystals. The reduced contributions of sampling fluctuations and fluctuations in the Čerenkov light yield would first and foremost manifest themselves in the performance for *electromagnetic* shower detection, since such fluctuations dominate the em energy resolution. We constructed two crystal matrices that were large enough

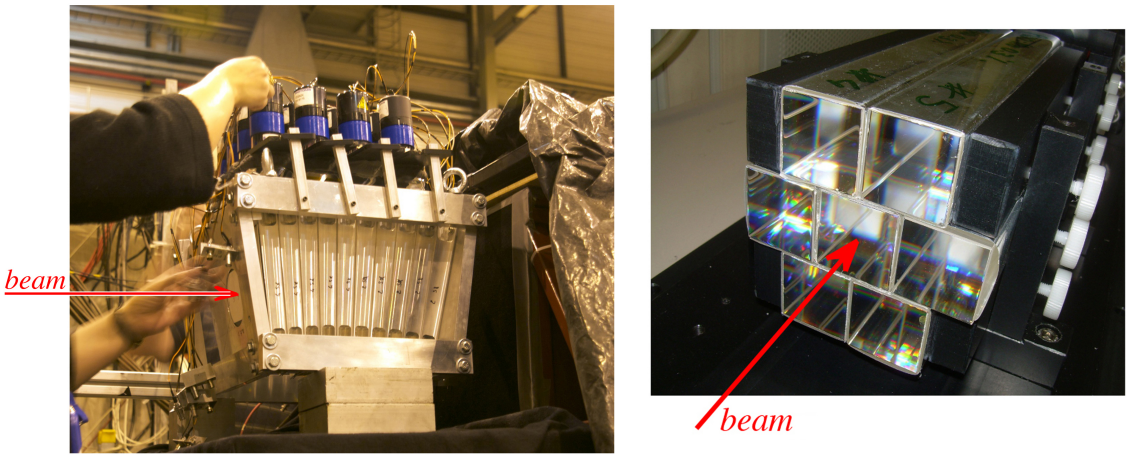

Figure 3: The 100-crystal BGO matrix (left) and the matrix of molybdenum doped $PbWO_4$ crystals (right) tested in the 2011 test beam campaign.

to contain high-energy electron showers (Figure 3). One matrix consisted of 100 BGO crystals used previously in the L3 experiment [3], the other one consisted of 7 custom made $PbWO_4$ crystals doped with 0.3% molybdenum. These detectors were instrumented in such a way that both scintillation and Čerenkov signals could be extracted from the light produced by showering particles. They were tested in electron beams with energies ranging from 4 - 180 GeV in the H8

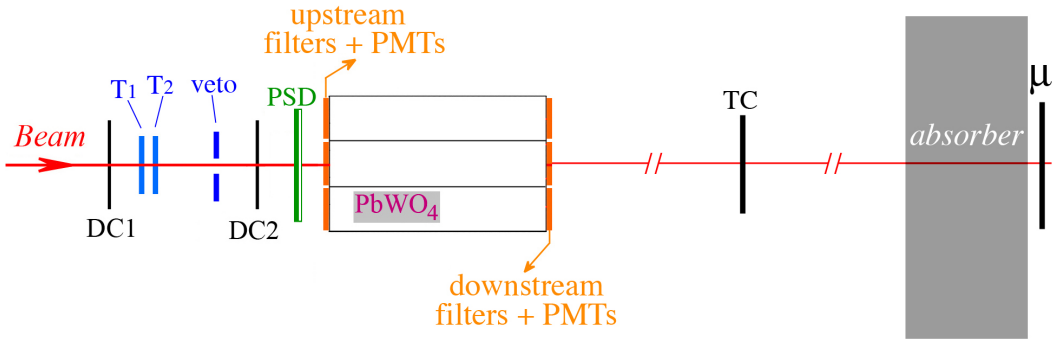

Figure 4: Experimental setup in which the $PbWO_4$ crystal matrix was tested (not to scale).

beam. The setup is schematically shown in Figure 4.

All practical methods that allow splitting the light produced in the crystals into sufficiently pure Čerenkov and scintillation components require optical filtering. Figure 5 illustrates how this can be successfully done in the case of the Mo-doped $PbWO_4$ crystals.

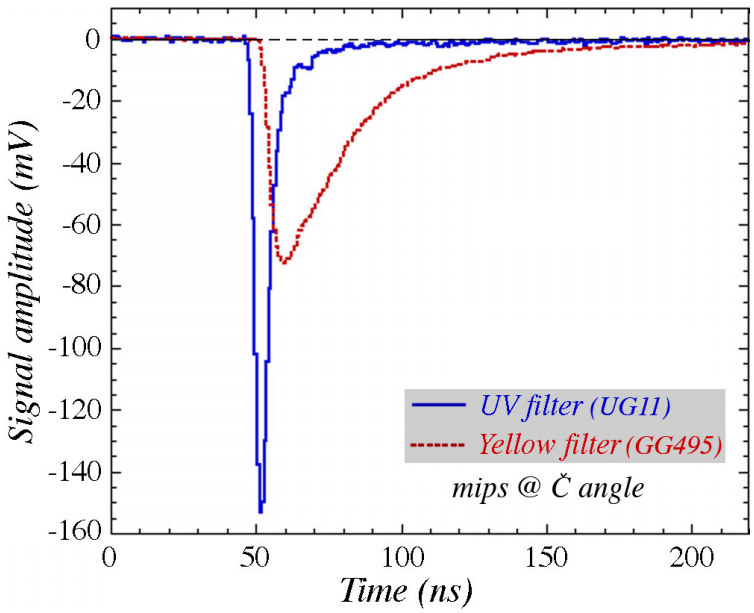

Figure 5: Average time structure of the signals from a single Mo-doped $PbWO_4$ crystal, placed at an angle of 60° with the beam line. The light produced by the particles traversing this crystal was filtered with UG11 and GG495 filters, respectively.

The choice of the filters turned out to be crucially important for the performance of the matrix as a dual-readout em calorimeter. In order to obtain good-quality Čerenkov signals, one has to select light with short wavelengths. However, this light is quite strongly attenuated because of self absorption in the crystal. To alleviate the effects of this on the energy resolution and the signal linearity, one can read the signal from both the upstream and downstream crystal faces and add the two results. The beneficial effects of this for the signal linearity are illustrated in Figure 6. However, if the crystal is read out from both ends with a filter intended to select the Čerenkov light, one has to find an alternative way to also extract a scintillation signal. We achieved this by using on one side a filter (U330) that only transmitted Čerenkov light, and on the other side a filter (UG5) which also transmitted some fraction of the longer wavelength light. The scintillation component in the latter signal could be extracted because of the different time structures of the two components (see Figure 5). The energy resolution measured for the Čerenkov signals is shown as a function of energy in Figure 7. Measurements were carried out for filter combinations U330/U330 (20 - 180 GeV) and for filter combination U330/UG5 (4 - 50 GeV). The results are well described by $E^{-1/2}$ scaling, except for a small deviation at low energies, where baseline fluctuations in the DRS readout module affected the resolution for the (small) signals. The results also show that the additional light transmitted by the UG5 filter led to an improvement in the resolution, indicating that this resolution is clearly limited by photoelectron statistics.

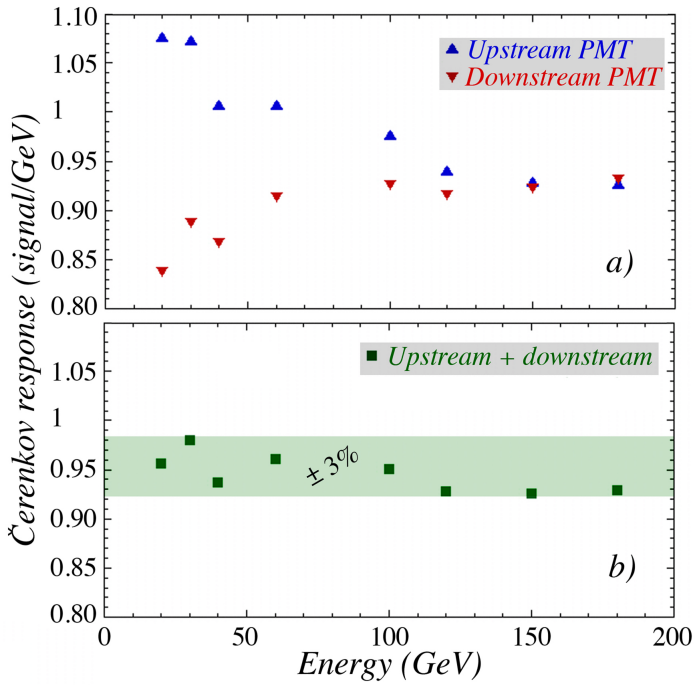

Figure 6: Signal linearity for electrons detected in the Mo-doped $PbWO_4$ crystal matrix. Shown is the response as a function of the electron energy for the Čerenkov signals. The matrix was equipped with U330 filters, both at the upstream and downstream end faces. The signals measured at both ends are both shown separately (a) and added together (b).

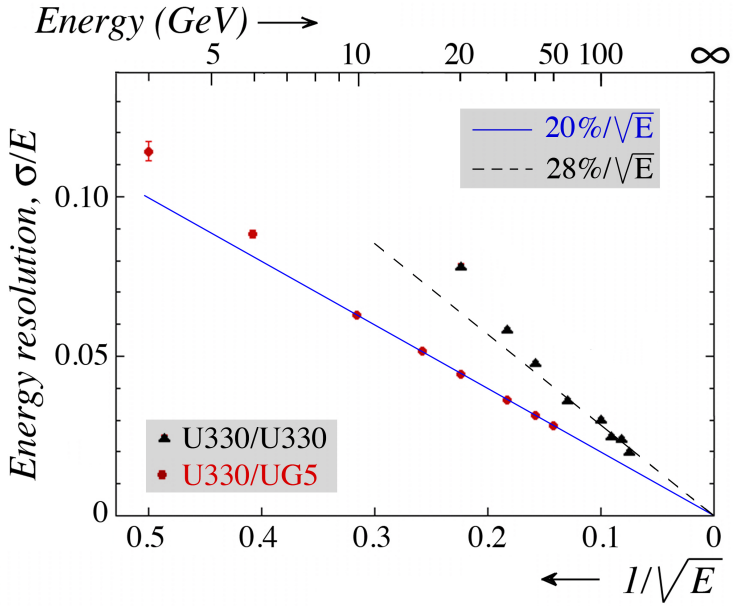

Figure 7: Energy resolution for electrons showering in the $PbWO_4$ crystal matrix, as a function of energy. The data points concern the resolution measured for the Čerenkov signals, derived from UV-filtered light detected at both ends of the crystal matrix. See text for details.

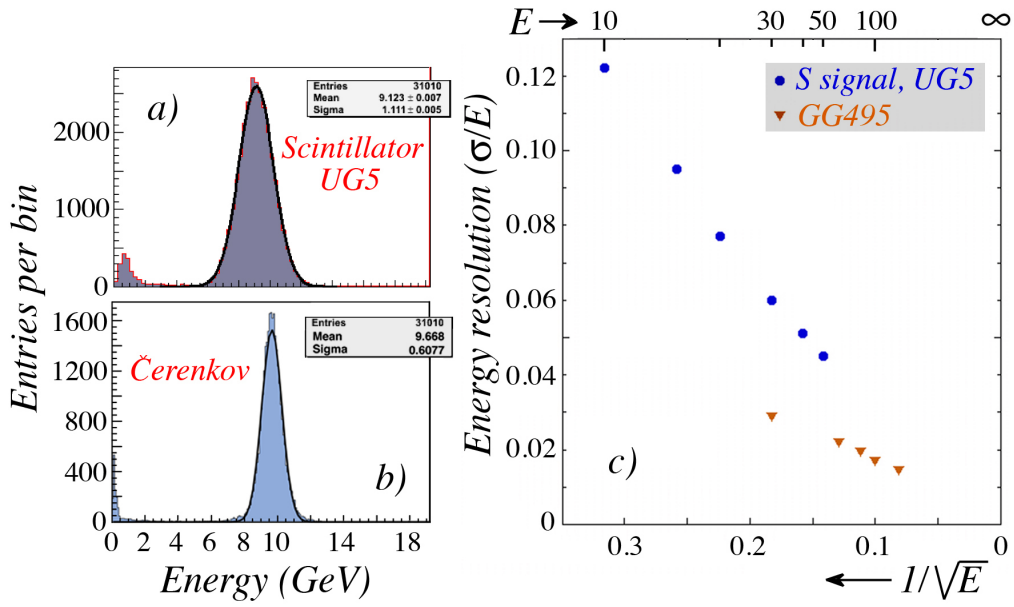

Figure 8: Signal distributions for the scintillation (a) and Čerenkov (b) components of the light generated in the $PbWO_4$ matrix by 10 GeV electron showers and filtered with the U330/UG5 combination. The energy resolution of the scintillation signal is compared with that obtained with the yellow (GG495, see Figure 5 filter in diagram c.

The performance of the $PbWO_4$ matrix for scintillation signals with the filter combination is illustrated in Figure 8. In diagrams a and b, typical signal distributions for 10 GeV electrons in the scintillation and Čerenkov channels are compared. Figure 8c shows the effect of filtering the light to favor the Čerenkov content of the signals on the energy resolution in the scintillation channel.

We determined the Čerenkov light yield in the U330/UG5 filter combination to be $\sim$ 25 photoelectrons per GeV deposited energy. This is less than what we have achieved in our fiber sampling calorimeters. The reason for this difference is the fact that, in order to extract sufficiently pure Čerenkov signals, we have to sacrifice a large fraction of the potentially available Čerenkov light. In addition, the light that does contribute to the Čerenkov signals is strongly attenuated, because of the absorption characteristics of the crystals. As an aside, we mention that these characteristics also make crystal-based dual-readout calorimeters probably quite prone to radiation damage. Our tests of the BGO crystal matrix led to similar conclusions.

Based on our experience so far, using crystals in combination with filters does not seem to offer a substantial benefit in terms of the Čerenkov light yield in dual-readout calorimeters. But we cannot exclude that other types of crystals, unknown to us, are better suited for this purpose.

3.1 Polarization measurements

One of the reasons why the Čerenkov light yield is so small in the crystal calorimeters discussed above is the very poor acceptance for Čerenkov light produced in em shower development in the setup in which they were tested (Figures 3,4). Only Čerenkov light produced in the late stages of the shower development, where the shower particles have "forgotten" the direction of

incidence of the beam particles, contribute to the signals. This became clear from a separate study in which we investigated the polarization of the light produced in a BSO crystal as a function of the depth inside developing em showers. Figure 9 shows the setup in which this

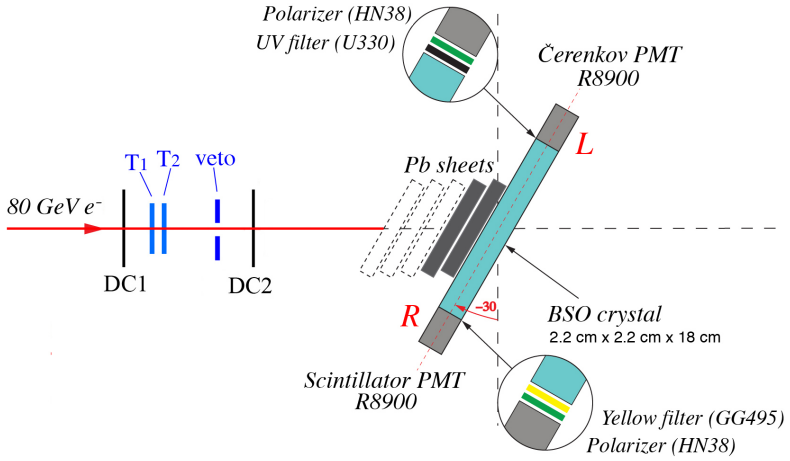

Figure 9: Experimental setup in which the polarization beam tests were performed (schematic and *not* to scale).

study was carried out. The BSO crystal was placed at an angle of 60° with the beam direction, optimizing the collection of Čerenkov light at the end face labeled L. A U330 filter was used to select the Čerenkov component. On the other end face of the crystal (labeled R), a GG495 filter selected the scintillation light. On both end faces, a polarizing filter was installed as well. As we showed in an earlier paper, rotating the latter filter over 90° changed the strength of the Čerenkov component by about a factor of four in the case of a beam of minimum iozing particles [11]. In the new measurements, a certain amount of lead was installed upstream of the crystal. By varying the thickness of this lead, the polarization characteristics of the detected light could be studied as a function of the depth inside the em shower that developed in this arrangement.

Figure 10 shows one result of these studies. The ratio of the detected signals on the R and L sides of the crystal is plotted as a function of the amount of lead installed upstream of the crystal, both for the favorable and unfavorable orientations of the polarization filter. The polarized light is concentrated in the early stages of the shower development and (surprisingly) beyond the shower maximum where the energy deposit is dominated by Compton scattering. This result suggests that the e^+e^- pairs produced abundantly in the early stages of the shower development as a result of the conversion of bremsstrahlung γs contribute very little to the production of Čerenkov light, and that this light is dominated by the excess negative charge due to the incoming beam particle in the early stage of the shower development and to Compton electrons dominating the energy deposit beyond the shower maximum. We will spend some beam time in 2012 to further test this hypothesis, which has potentially interesting applications.

4 The SuperDREAM fiber calorimeter

After extensive tests of many details, the RD52 Collaboration has embarked on the construction of the new full-scale fiber calorimeter, which should significantly improve the performance of

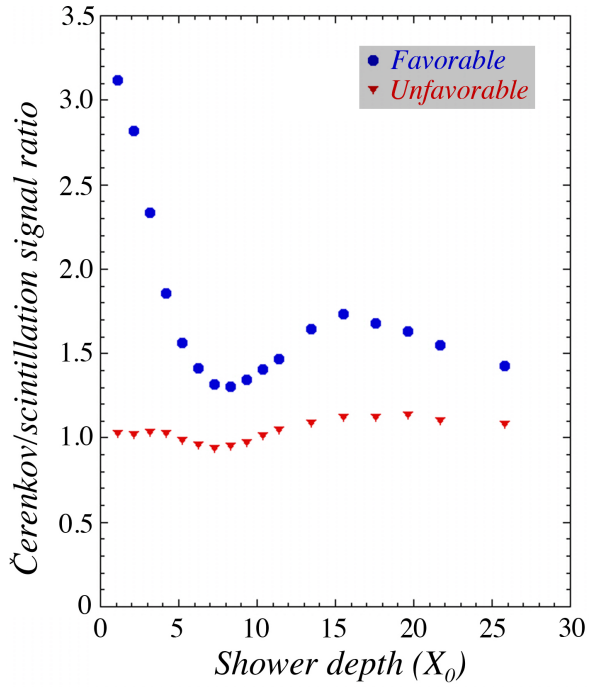

Figure 10: Ratio of the 80 GeV e^- Čerenkov and scintillation signals measured in PMT L, as a function of the amount of lead the beam particles traversed before entering the crystal. Results are given separately for the favorable and unfavorable orientation of the polarizing filter for detecting Čerenkov light.

the original 1-ton DREAM module. This detector will be large enough to contain high-energy hadron showers at a sufficient level to eliminate the effects of leakage fluctuations, which dominated the energy resolution of the original DREAM module. After fluctuations in em shower content are eliminated with the dual-readout method, the hadronic energy resolution of this fiber calorimeter is then dominated by sampling fluctuations and fluctuations in Čerenkov light yield. We aim to reduce both sources of (Poisson) fluctuations to about $10\%/\sqrt{E}$. In that case, the hadronic energy resolution ($\sim 20\%/\sqrt{E}$) will approach the theoretical limit, while electrons and γs should be detected with resolutions of $\sim 10\%/\sqrt{E}$. These improvements are achieved by making the following modifications to the original DREAM fiber module:

- Fibers are individually embedded in the absorber structure, instead of in groups of seven
- The packing fraction of the fibers is roughly doubled
- The numerical aperture of the Čerenkov fibers is increased
- The upstream end of the Čerenkov fibers is aluminized
- The quantum efficiency of the photocathode is increased (using Super Bialkali PMTs)

Another important difference with the original DREAM fiber calorimeter concerns the readout, which is based on a Domino Ring Sampler (DRS) circuit that allows time structure measurements of each signal with a sampling rate of 5 GHz (0.2 ns time resolution). We have shown

previously that detailed measurements of the time structure are an invaluable source of information, not only for separating the Čerenkov and scintillation signals from crystals, but also to identify and measure the contribution of neutrons to the scintillation signals [13]. Another important goal of the time structure measurements is to determine the depth at which the light is produced in this longitudinally unsegmented calorimeter. To this end, we plan to make use of the fact that the light signals travel at a slower speed in the fibers ($\sim$ 17 cm/ns) than the particles producing this light (30 cm/ns). And finally, thanks to the aluminized upstream ends of the Čerenkov fibers, the time structure measurements will give us important additional tools to identify electrons in this unsegmented calorimeter. Details of the proposed detector development program are described in [1].

4.1 Current activities

The fiber calorimeter is modular. The modules are being constructed in Pavia and Pisa. Each module contains 4 towers, and is read out by 8 PMTs, 4 for the Čerenkov channels and 4 for the scintillation channels. Each module is 2.5 m long (10 $\lambda_{\rm int}$), has a cross section of 9.3×9.3 cm^2 and a fiducial mass of about 150 kg. The first modules were constructed with lead as absorber material. Now, also the first copper module is nearing completion. In 2012, we hope to complete 4 copper modules and 9 lead ones. Figure 11 shows pictures of the first (lead-based) module that was built. This module was extensively tested in the H8 beam, with the purpose to obtain important input for the final design parameters. The analysis has concentrated on the following characteristics:

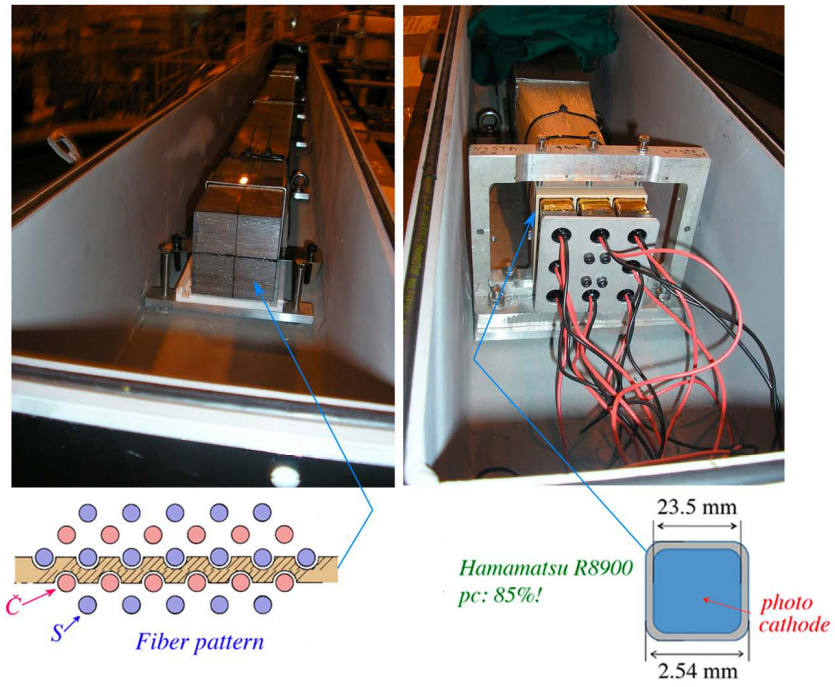

Figure 11: A module of the new SuperDREAM fiber calorimeter.

- The Čerenkov light yield
- The attenuation characteristics of the fibers
- Measurement of the depth of the light production with the DRS information

For the Čerenkov light yield, we measured 32 photoelectrons per GeV deposited energy. For copper absorber, one may naively expect this light yield to be larger because of the suppression of the em response in high-Z absorber material ($e/mip \sim 0.6$). Yet, it would still be significantly less than what we aim for. The main culprit for this difference is Rayleigh scattering at $\lambda < 500$ nm in polystyrene, the core material of the clear fibers used in this module. This feature also limited the attenuation length of the clear fibers to ~ 6 m. For this reason, we decided to switch to PMMA fibers for detecting the Čerenkov light. Bench tests have shown that the effect of a smaller numerical aperture (0.50 instead of 0.72) is more than offset by the decreased light absorption in the short-wavelength region that dominates the Čerenkov spectrum.

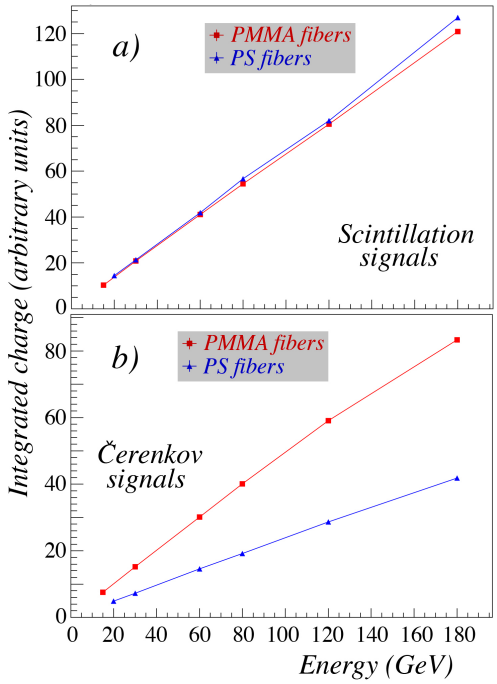

Figure 12: Average signal as a function of the energy deposited by showering electrons in the first two modules of the new SuperDREAM fiber calorimeter, for the scintillation (a) and the Čerenkov (b) signals. The scintillating fibers were the same in both modules, but the clear plastic fibers were based on polystyrene in the module constructed in Pisa and on PMMA in the module constructed in Pavia. The same PMT were used for detecting the signals in both modules.

Measurements with the second, also lead-based module, confirmed this. Figure 12 shows the average signals for the two modules, as a function of the energy of the beam electrons that generated these signals. Exactly the same PMTs, operating at exactly the same voltage levels, were used to measure these signals. The figure shows that the scintillation signals (Figure 12a)

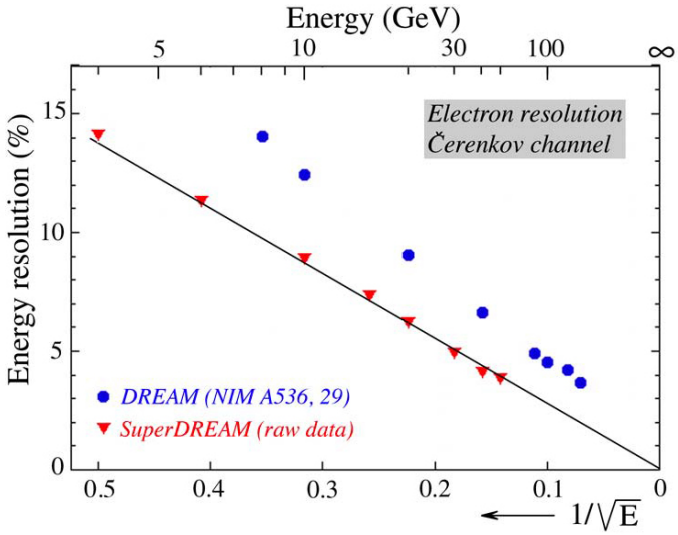

Figure 13: Comparison of the em energy resolution in the Čerenkov channel, measured with the first SuperDREAM modules and with the original DREAM calorimeter [14].

were indeed the same in these two modules. However, the change from polystyrene to PMMA based clear fibers increased the Čerenkov signals by about a factor of two (Figure 12b).

The changes in the structure of the fiber module did indeed pay off in the form of a substantially improved em energy resolution. This is illustrated in Figure 13, where this resolution is compared to the published values obtained with the original DREAM module [14]. The improvement is especially important at the highest energies, due the absence of a significant deviation from $E^{-1/2}$ scaling (the so called "constant term"). Further improvements may be expected as a result of the use of copper absorber, fiber aluminization and better shower containment.

Figure 14: The setup in which individual SuperDREAM modules are being tested in the H8 beam. The module is contained in a box surrounded by 16 leakage counters.

Improved shower containment is of course much more important for hadron showers. Most of the energy leaking out of a cylinder with a radius of $\sim 10\rho_M$ is carried by neutrons. We have build a very low-cost instrument to detect these neutrons. It consists of 10 cm thick plastic scintillator plates, made into 50×50 cm^2 modules that surround the fiber calorimeter. Figure 14 shows one fiber module surrounded by 16 such neutron counters. These counters were calibrated by lining up all 16 of them in a muon beam, as illustrated in Figure 15.

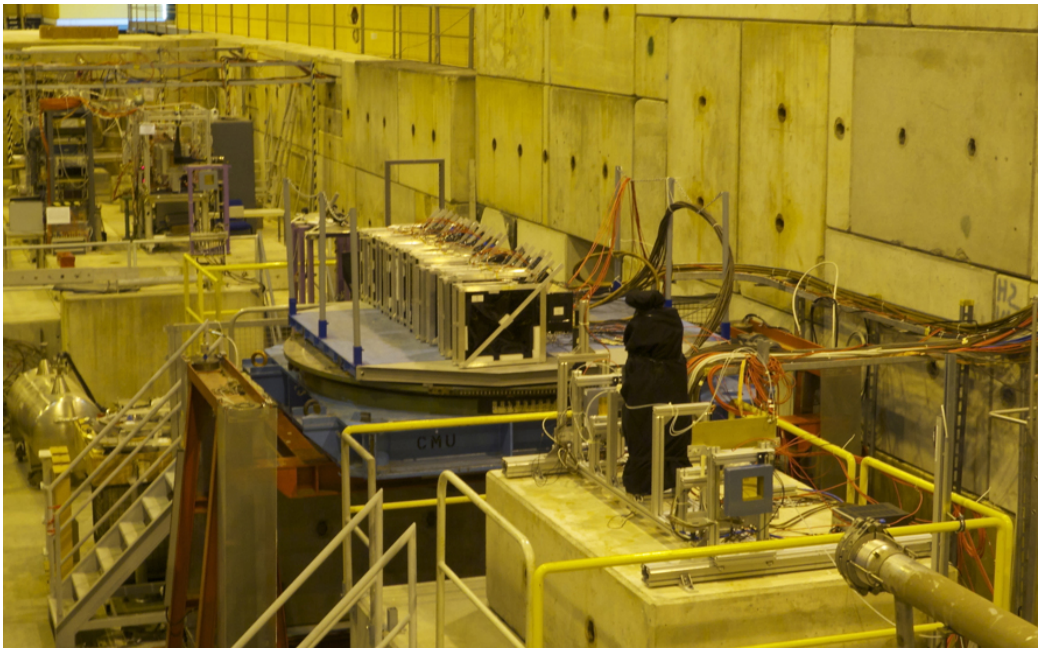

Figure 15: All 16 leakage counters are lined up to be calibrated with muons.

We tested the performance of this neutron shield by exposing the system shown in Figure 14 to a beam of high-energy hadrons, 180 GeV π^-. Results are shown in Figure 16. The signal distribution measured with the scintillating fibers (Figure 16a) exhibits the characteristics typical for poor hadron calorimeters, in particular the asymmetric line shape and the large width, $\sigma_{\rm rms}$/mean = 27%. Figure 16b shows that this scintillation signal is anti-correlated with the total signal registered in the neutron counters, which confirms that the latter are indeed doing the job they are expected to do, since a larger scintillation signal implies that a larger fraction of the total shower energy is carried by the em (π^0) shower component, in which nuclear reactions play no significant role. The dual-readout aspects of this system are featured in Figure 16c, which shows that the scintillation signal (including the contributions from the leaking neutrons) is anti-correlated to the Čerenkov/scintillation signal ratio. This ratio, which is measured for each individual event, is a measure of the em shower fraction. It can be used in a straightforward way to translate the measured scintillation signal into the energy of the showering hadron, by basically calculating what the scintillation signal would have been if the em fraction had been 1.0, as in electron showers. The result of this operation is shown in Figure 16e. The signal distribution is much more narrow, centered around the correct value, and well described by a Gaussian function. The resolution has improved to about 5%. This result, which is very

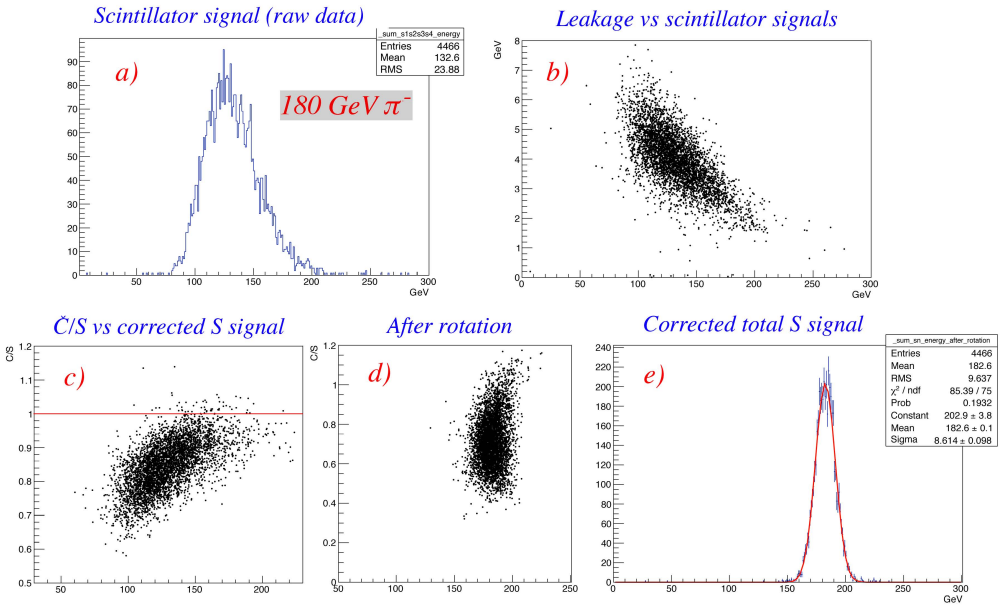

Figure 16: First measurements of pions in a single module of the new SuperDREAM fiber calorimeter, surrounded by leakage detectors. See text for details.

encouraging, may be expected to improve further when the fiber calorimeter is enlarged, and the energy leaking out of the central module is measured more precisely.

The preference for copper as absorber material derives, apart from the higher e/mip value and the expected larger Čerenkov light yield for showers associated with that, also from the fact that the mass per $\lambda_{\rm int}^3$ is almost a factor two smaller than for lead. This means that calorimeters, in order to contain hadron showers at the required level, can be much less massive when Cu absorber is used. The fact that $e/mip \sim 0.9$ and not 0.6 as in lead (Figure 17a) also means much better linearity for hadrons with momenta $\lesssim 5$ GeV/c [15, 16]. Such hadrons form an important component of jets, even at very high energies. The non-linearity measured with the compensating ^{238}U/plastic-scintillator ZEUS calorimeter (Figure 17b) may illustrate the importance of the latter effect.

It has turned out to be non-trivial to produce copper profiles with the tolerance level required for our application. However, thanks to the persistence of some of our collaborators, this problem has been solved, and the first copper module is nearing completion. Figure 18 shows some pictures of this module.

Thanks to the modular structure of the calorimeter, which makes it possible to rearrange the modules in different matrices, and to the fact that a large fraction of the shower energy

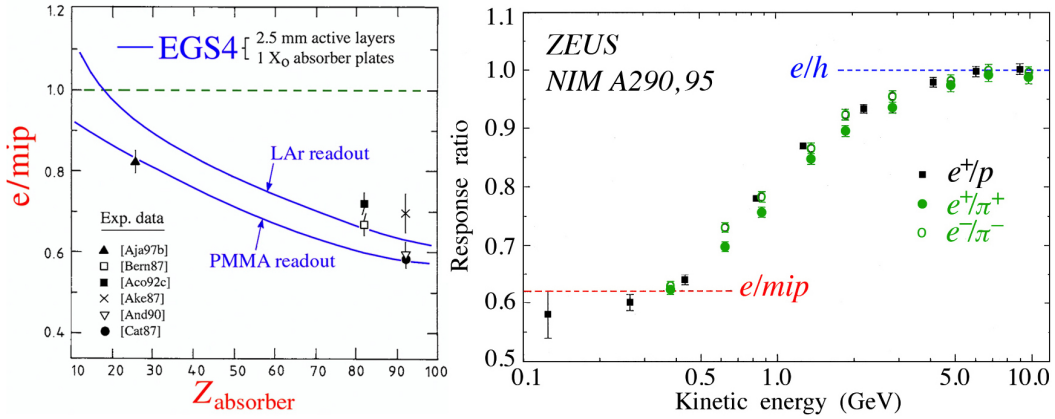

Figure 17: The response ratio for em showers and minimum ionizing particles in sampling calorimeters as a function of the Z value of the absorber material [15] and the consequences of this ratio on the response of the ZEUS calorimeter to low-energy hadrons [16].

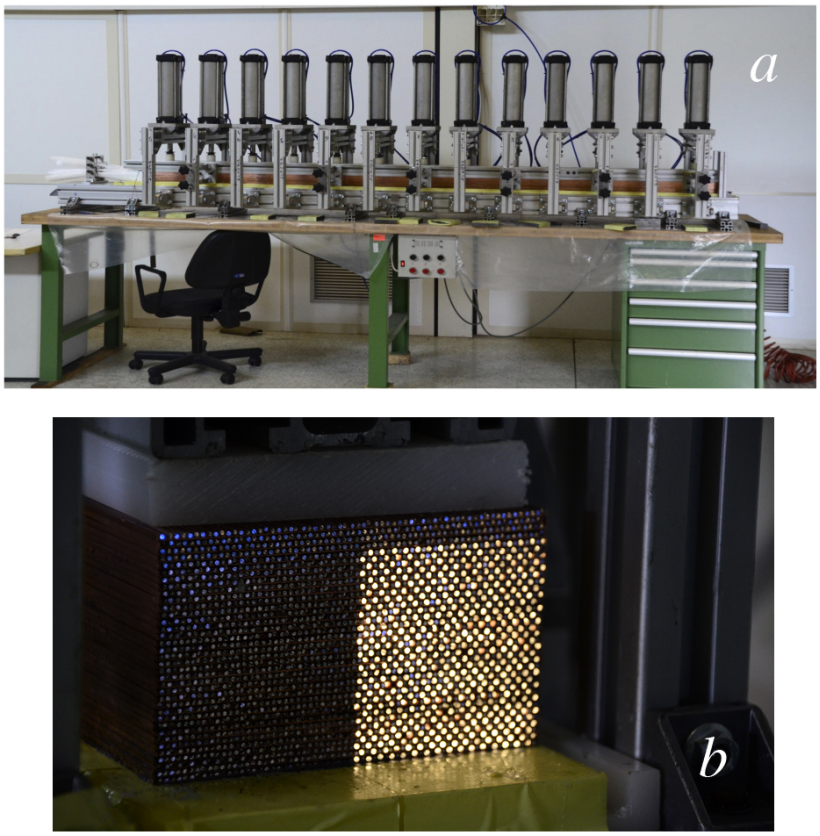

Figure 18: The first SuperDREAM module made with copper absorber, under construction in Pisa. Shown are an overview of the assembly area, where the 2.5 m long grooved copper plates are pressed together and bonded with minimal glue (a), and a front view of the 512 undoped fibers in one of the 4 towers comprising this module (b). The latter picture was taken by illuminating the fiber bunch from the rear end. The (non-illuminated) scintillating fibers are vaguely visible as blue dots in between the undoped ones.

is deposited in a relatively small area, we will be able to make detailed comparisons of the performance of copper-based and lead-based structures, both for electromagnetic and hadronic showers.

The beam tests of our first (non-aluminized) SuperDREAM modules also produced valuable information on the performance of the DRS readout. Figure 19a shows the distribution of the time difference between the PMT signals from 80 GeV electrons measured in the calorimeter and the trigger counters upstream. This difference was obtained by measuring the start of the calorimeter signals with the DRS chip, where the domino wave was started by the trigger signal. We see that a time resolution of 0.55 ns is achieved in this way. The same measurement for 180

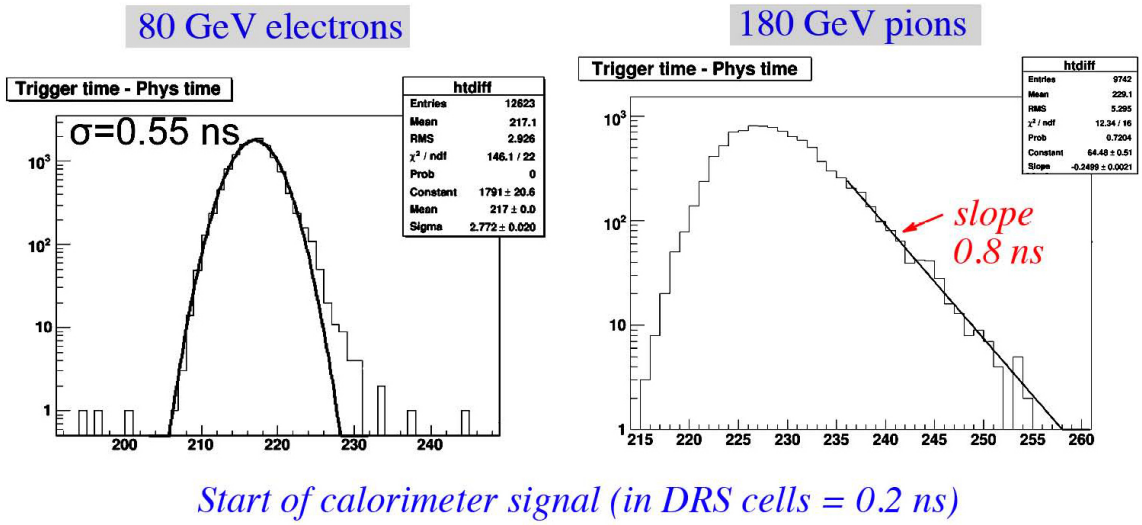

Figure 19: The starting time of signals from 80 GeV electron (a) and 180 GeV pion (b) showers in a SuperDREAM module, measured with the DRS readout. The readout was triggered by the passage of a beam particle through the upstream trigger counters.

GeV pions yielded a very different time distribution. The slope of 0.8 ns reflects the fact that the light is produced at a depth z which varies like $\exp -z/\lambda_{\rm int}$. Since the interaction length $\lambda_{\rm int} \sim 25$ cm in this detector, the time resolution of 0.55 ns means that the depth at which the light is produced can be determined with a precision better than 20 cm in this way. We expect that aluminized fibers will make it possible to further improve this precision.

We checked that the starting time of the DRS signals indeed measures the depth at which the light is produced in the fibers, by comparing the DRS information with the depth measured in two other ways, namely from the longitudinal profile measured in the leakage counters (Figure 20a) and from the lateral displacement of the center-of-gravity of the calorimeter signals with respect to the coordinates measured in the upstream wire chambers (Figure 20b). Both comparisons confirm the correctness of our conclusions.

4.2 Near-term plans

In 2012, we are planning to focus our attention and resources on the following issues:

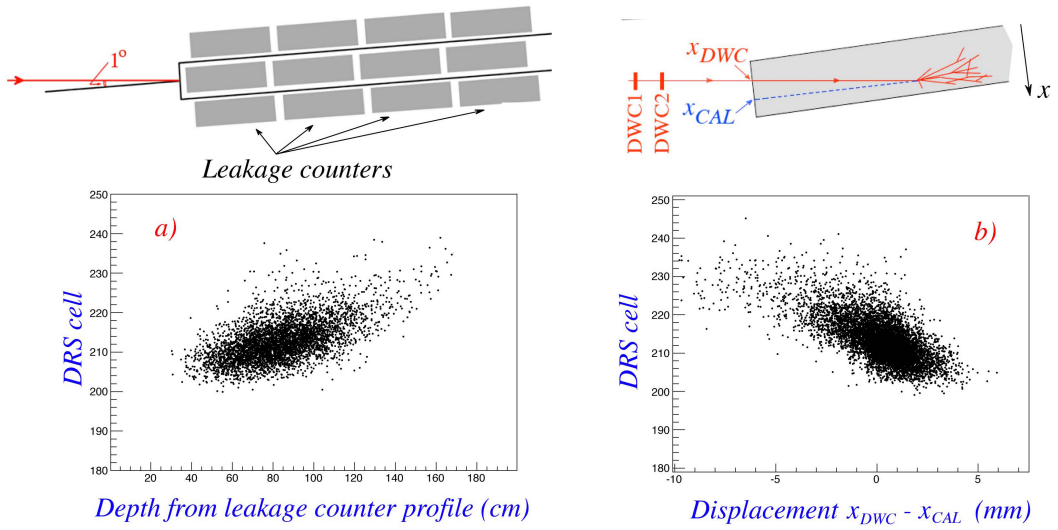

Figure 20: The depth of the light production in the unsegmented SuperDREAM fiber module versus the depth measured from the leakage profile (a) or from the displacement of the center-of-gravity with respect to the coordinates measured in the upstream wire chambers (b).

- Aluminizing the fibers intended for detecting the Čerenkov signals. We have received a batch of about 2000 fibers that were aluminized by E. Hahn at Fermilab. These fibers will be installed in one of the modules currently under construction. We are planning to study the effects of these fibers on the performance of our calorimeter in great detail in this year's beam tests. We are also in contact with a group from LIP Lisbon, who are experienced in this type of work (they aluminized all the fibers of the ATLAS TileCAL) and have expressed interest in joining RD52.

- Improvement of the signal linearity and reduction of the electronic noise. Based on the results of our electron measurements done in 2011, we have redesigned the base of our PMTs. This should reduce/eliminate the space charge problems that limit the dynamic range over which the calorimeter is linear. Careful inspection of the entire readout/DAQ chain, systematically removing sources of ground loops, has already reduced the noise levels by a factor of two. This noise is responsible for deviations from $E^{-1/2}$ scaling at low energies (see Figure 7). We intend to obtain further reductions of the noise levels in 2012.

- Construction of the SuperDREAM fiber calorimeter. We expect to finish 13 modules in 2012, and hope to be able to test the assembled detector, including its neutron shield, extensively before the CERN accelerators shut down for a major LHC upgrade in 2013. Several configurations of copper and lead based modules will be assembled and tested for this purpose.

- The system of leakage counters will be completed. In total, we are planning to build 40 counters. The total leakage detector will have a mass of more than one ton.

- Monte Carlo simulations of the detector configurations described above.

4.3 Plans for the longer-term future

Plans for 2013 and beyond include the following:

- Completion of the construction of the 5-ton SuperDREAM calorimeter module
- Testing this calorimeter in stand-alone mode, and in combination with an em dual-readout calorimeter consisting of crystals. Currently, we have two crystal matrices that could be used for this purpose, namely a 100-crystal matrix consisting of refurbished BGO crystals from the L3 experiment, and a 7-crystal matrix of molybdenum doped $PbWO_4$ crystals that was specifically developed for our purpose. We are also considering further extending this matrix and/or building a new one out of BSO crystals.
- Development of absorber structures with considerably higher density. This would make it possible to construct more compact calorimeters of this type. Even though the cost of these new structures is likely to be much higher, this may lead to important overall savings. For example, a 10 m long barrel calorimeter with an inner radius of 1 m would encompass an instrumented volume of about 350 m^3. This could be reduced to 180 m^3 if tungsten were used as absorber material instead of copper.
- Studies of projective calorimeter structures based on the DREAM concept. If a calorimeter of the SuperDREAM type was chosen for a 4π experiment, a projective geometry would be required. This poses a number of complications, which are however not unsolvable. In the context of the RD1 and RD25 projects, fully projective fiber calorimeters have been built [17, 18]. We plan to build on the expertise developed in that context.
- Development of an alternative readout system. Splitting the thousands of fibers sticking out of the back, separating them into scintillating and Čerenkov ones and bunching them accordingly is very cumbersome. Moreover, this system takes up valuable space (≈ 50 cm in the detectors we have built so far), and the fiber bunches may sometimes act as antennas, picking up signals that have nothing to do with the ones for which they are intended. For this reason, we have started to look into a readout system based on silicon photomultipliers. The fibers would no longer stick out of the back, but each fiber would be connected to its own individual SiPM, located at the end face of the absorber structure. Given the large surface area that would have to be covered, such a system is at present still prohibitively expensive. However, given the rapid development of this technology, this might change in the years to come. We are in any case planning to test this idea on a modest scale.

5 Requested CERN support

Of course, the plans described in the previous section can only be carried out if our funding agencies provide the means for it. This in turn will depend on the results of future beam tests. In that sense, the support from CERN is of crucial importance.

We would like to request that CERN make some resources available, particularly in the form of support for carrying out our program of beam tests. A modest account from which crane operations, help from technicians in the workshop of Experimental Hall 887, nuts and bolts from the CERN stores, *etc*. could be covered would be highly appreciated. For some of our collaborators, RD52 is the only CERN activity in which they are involved. A dedicated RD52 office in the North Area would be very helpful for them, and for the Collaboration as a whole.

References

[1] DREAM Collaboration (Wigmans R) 2010, CERN-SPSC-2010-012/SPSC-M-771.

[2] Akchurin N *et al.* 2005, Nucl. Instr. and Meth. in Phys. Res. **A537**, 537.

[3] Adeva B *et al.* 1990, Nucl. Instr. and Meth. in Phys. Res. **A289**, 35.

[4] Lewandowski B 2002, Nucl. Instr. and Meth. in Phys. Res. **A494**, 303.

[5] Miyabayashi, K 2002, Nucl. Instr. and Meth. in Phys. Res. **A494**, 298.

[6] CMS Collaboration, Journal of Instrumentation **5** (2010) T03011.

[7] Akchurin N *et al.* 2007, Nucl. Instr. and Meth. in Phys. Res. **A582**, 474.

[8] Akchurin N *et al.* 2008, Nucl. Instr. and Meth. in Phys. Res. **A595**, 359.

[9] Akchurin N *et al.* 2009, Nucl. Instr. and Meth. in Phys. Res. **A604**, 512.

[10] Akchurin N *et al.* 2010, Nucl. Instr. and Meth. in Phys. Res. **A621**, 212.

[11] Akchurin N *et al.* 2011, Nucl. Instr. and Meth. in Phys. Res. **A638**, 47.

[12] Akchurin N *et al.* 2011, Nucl. Instr. and Meth. in Phys. Res. **A640**, 91.

[13] Akchurin N *et al.* 2008, Nucl. Instr. and Meth. in Phys. Res. **A598**, 422.

[14] Akchurin N *et al.* 2005, Nucl. Instr. and Meth. in Phys. Res. **A536**, 29.

[15] Wigmans R 2000, *Calorimetry, Energy Measurement in Particle Physics*, International Series of Monographs on Physics, Vol. 107, Oxford University Press.

[16] Andresen A *et al.* 1990, Nucl. Instr. and Meth. in Phys. Res. **A290**, 95.

[17] Badier J *et al.* 1994, Nucl. Instr. and Meth. in Phys. Res. **A337**, 326.

[18] Anzivino G *et al.* 1995, Nucl. Instr. and Meth. in Phys. Res. **A357**, 350.